Electronic Supplementary Material (ESI) for Soft Matter.

Supplementary information

Responsive Soft Actuator: Harnessing Multi-Vapor, Light, and Magnetic Field Stimuli

Vipin Kumar[a,b] and Dillip K. Satapathy*[a,b]

[a]Soft Materials Laboratory, Department of Physics, IIT Madras, Chennai, India
[b]Center for Soft and Biological Matter, IIT Madras, Chennai-600036, Tamil Nadu, India
E-mail: dks@iitm.ac.in

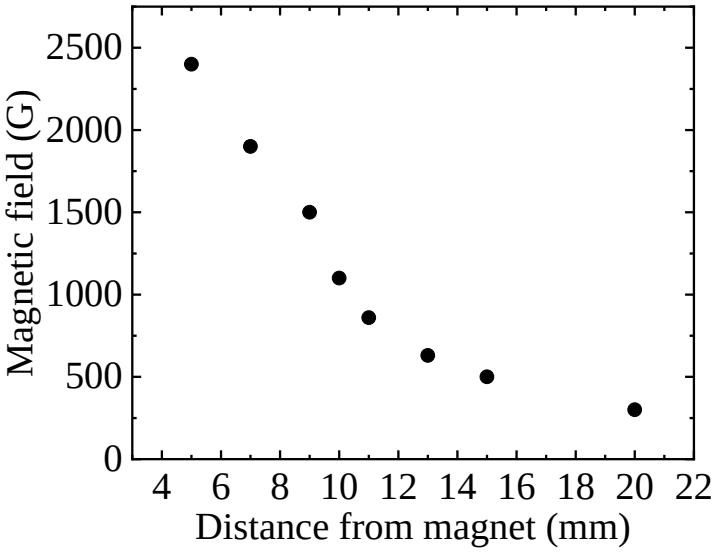

Figure S1: The magnetic field strength measured as a function of distance from the surface of the magnet. A circular permanent neodymium magnet (diameter = 20 mm, thickness = 10 mm) is used to produce the magnetic fields, and a Gauss meter is used to measure the field strength.

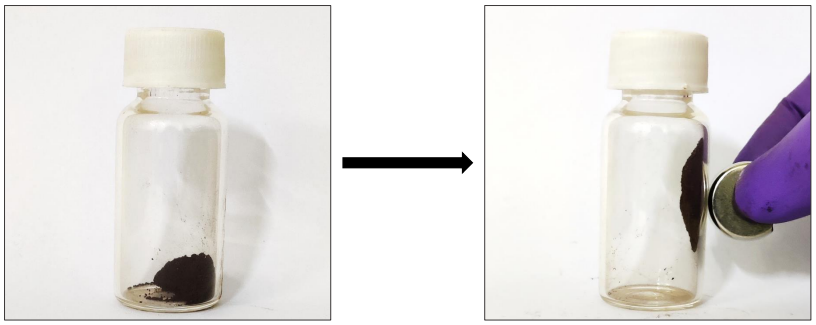

Figure S2: (Left side) Iron oxide nanoparticles are present at the bottom of the bottle in the absence of an external magnetic field. (Right side) The iron oxide nanoparticles are displaced and are attracted towards a permanent magnet held near the boundary of the bottle.

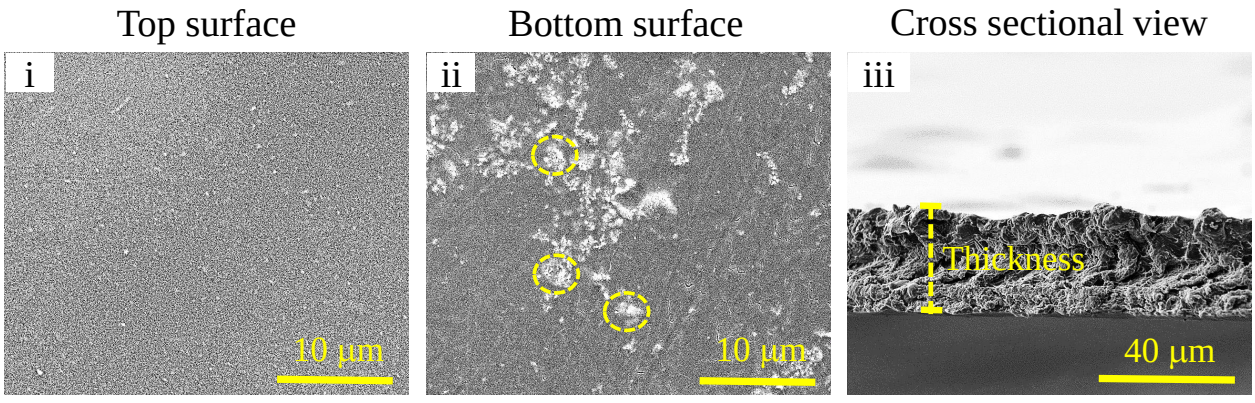

Figure S3: (i) The surface morphology of the composite film exposed to air during the drying process. (ii) The surface microstructure of the composite film in contact with the petri dish. The white region enclosed by dashed yellow lines shows the presence of nanoparticle clusters within the composite film. (iii) The cross-sectional view of the composite film, with the thickness of the film denoted by the dashed yellow line.

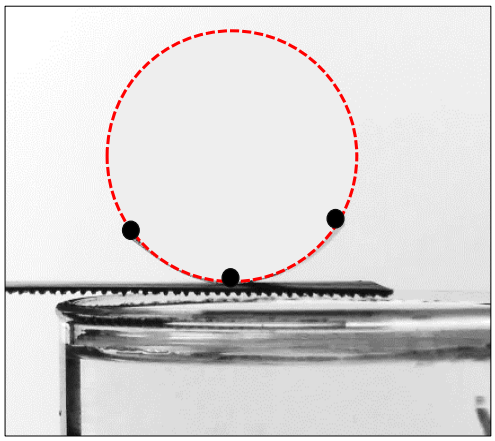

Figure S4: The bending curvature of the film upon exposure to the stimuli was calculated by tracing the three points on the film and fitting them into a circle. Here, the three black dots are three points traced on the film, and the red dotted circle is fitted on these three dots to calculate the bending curvature of the film.

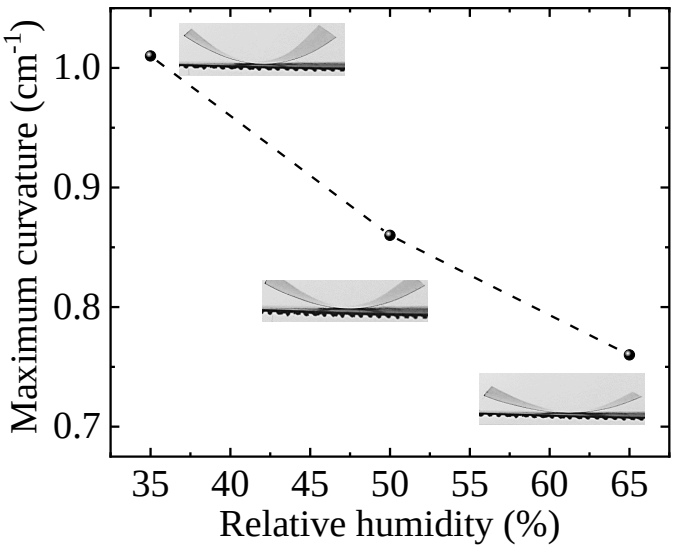

Figure S5: The maximum bending curvature values of the composite film upon exposure to the water vapor exposure from the bottom side at three different relative humidity values (35%, 50%, and 65%). The dimensions of the film: length = 20 mm, width = 16 mm, thickness = 23±1 μm.

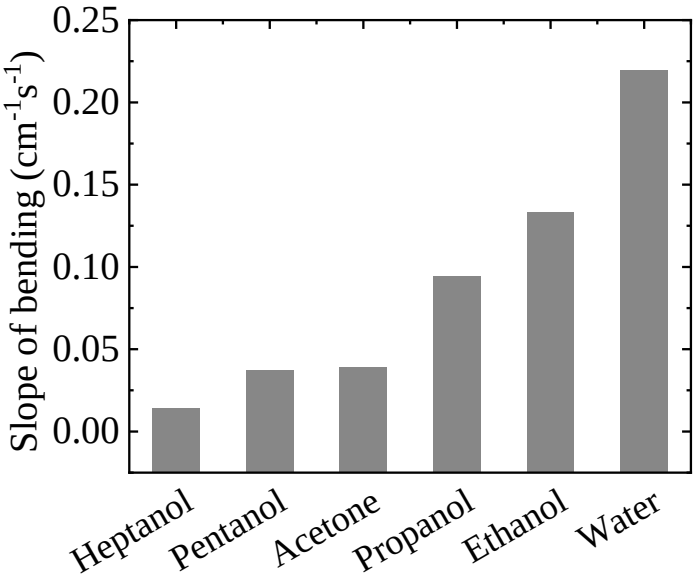

Figure S6: The slope of bending of the film upon exposure to different organic solvent vapors. The slope is minimum for heptanol and maximum for water vapor.

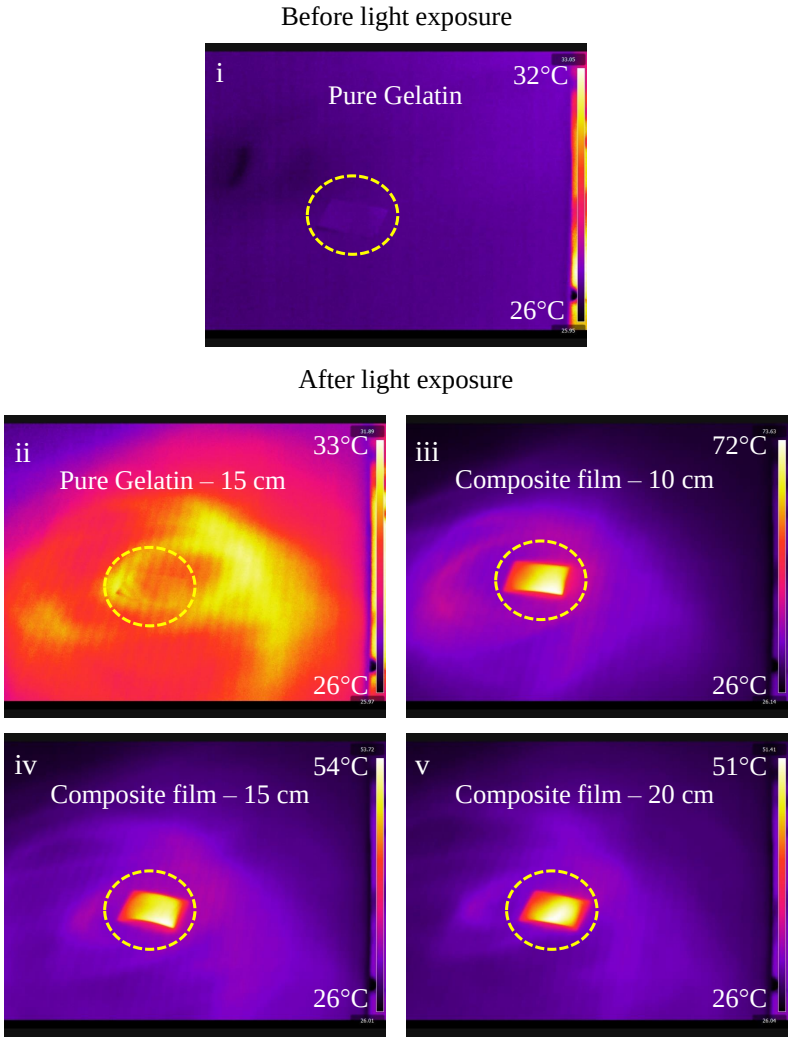

Figure S7: Thermal camera image of a pure gelatin film before (i) and after (ii) infrared light exposure. The film is marked inside the yellow dotted circle. Thermal camera images of the composite film after 2 seconds of exposure to the infrared light from different distances (iii) 10 cm, (iv) 15 cm, and (v) 20 cm. As the distance between the film and the light source increases, the surface temperature of the film decreases.

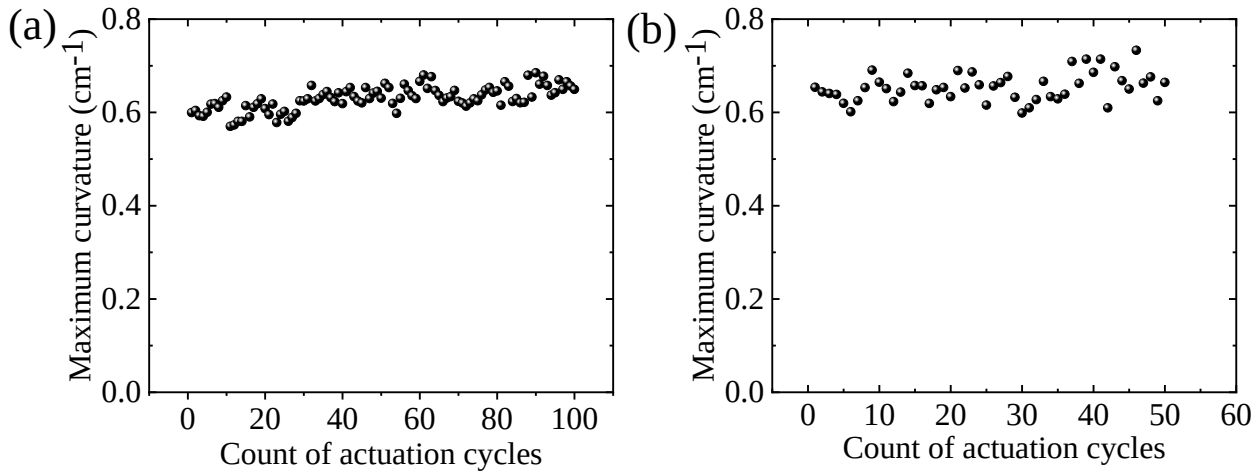

Figure S8: (a) The maximum bending curvature values of the composite film upon exposure to the water vapor from the bottom side for 100 cycles. The dimensions of the film: length = 20 mm, width = 16 mm, thickness = 26±1 μm. (b) The maximum bending curvature values of the composite film upon exposure to the infrared light from a distance of 15 cm for 2 seconds. The dimensions of the film: length = 20 mm, width = 12 mm, thickness = 25±1 μm.

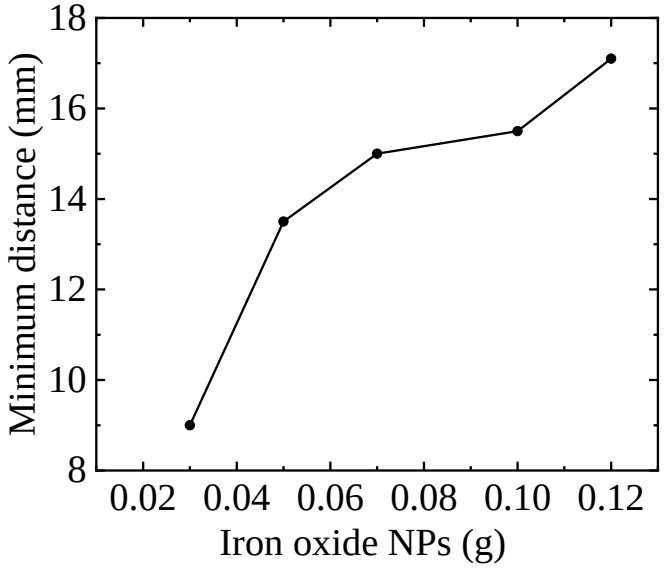

Figure S9: Maximum distance of attraction versus the amount of NPs in the film. As the concentration of NPs increases in the film, the maximum distance from which the film experiences an attraction also increases.

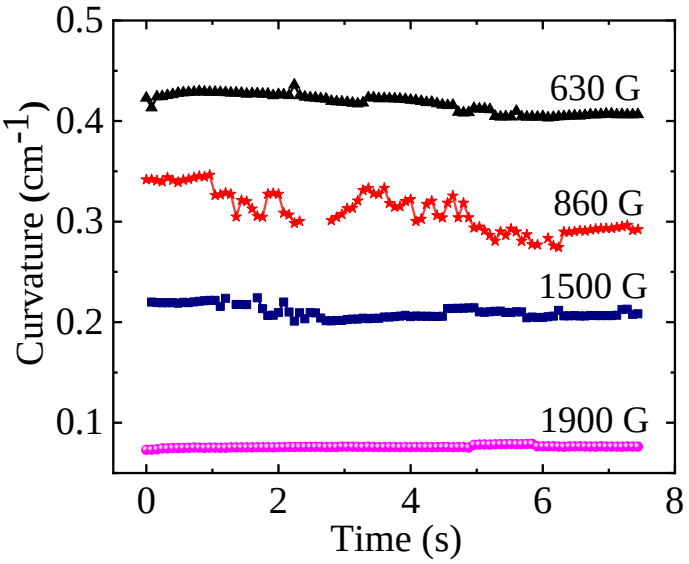

Figure S10: Bending curvature versus time during control over the actuation in water vapor by an external magnet. As the applied magnetic field increases, the bending curvature value decreases.

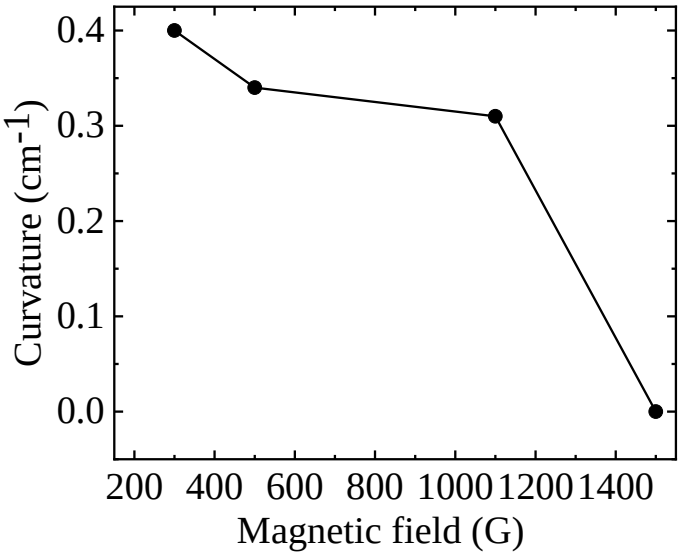

Figure S11: Plot shows as the applied magnetic field increases, the maximum bending curvature of the film decreases upon exposure to the light for 3 seconds.

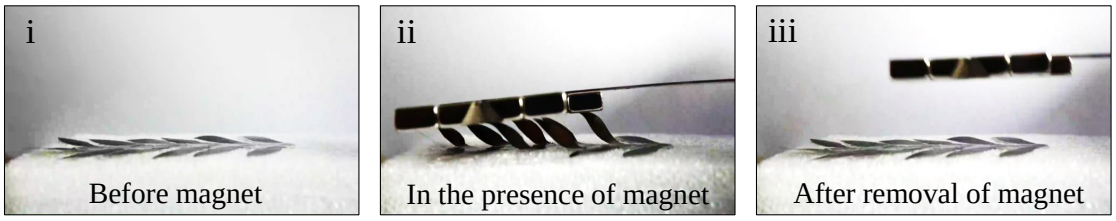

Figure S12: (i) The leaflets made up of the composite film in the absence of the magnetic field, (ii) the bending state of the leaflets in the presence of the external magnetic field, (iii) the leaflets return to their original state after removal of the external magnetic field.

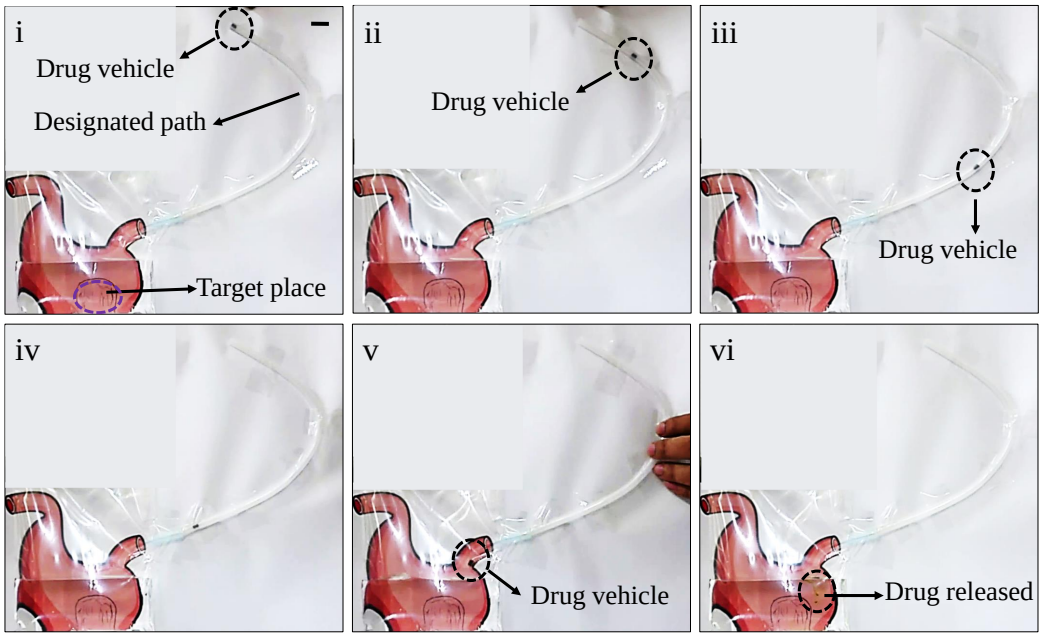

Figure S13: Drug delivery: First, the drug is placed in the hollow cylinder (drug vehicle) made up of composite film, (i) loaded vehicle inserted into a designated path, (ii), (iii) and (iv) drug vehicle is moving with the help of external magnetic field applied from the back side of the paper, which is just following the designated path, (v) drug vehicle just entered into the targeted place, (vi) the drug vehicle dissolves into the water and drug is released from the vehicle. The scale bar = 15 mm.

Table S1: Comparison table of published literature of multi stimuli-responsive soft actuators with our work

Sl. No.	**Materials**	**Response to Humidity**	**Response to Organic vapor**	**Response to Light/Magnetic field**	**Response time/ Structure**	**Control by magnetic field**	**Bidirectional actuation**	**Ref.**
1.	PVDF/LDPE	No	Yes	Yes/No	4 s (acetone)/ Bilayer	No	No	[1]
2.	MXene/polyethylene	Yes	No	Yes/No	NA/ Bilayer	No	No	[2]
3.	CNT-Nafion/polyethylene	Yes	Yes	Yes/No	NA/ Bilayer	No	No	[3]
4.	GO/ PMMA	Yes	No	Yes/No	5 s (humidity) and 20 s (light)/ Multilayer	No	No	[4]
5.	Chitosan/ PVA/ Azobenzene	Yes	No	Yes/No	20 s (humidity) and 50 s (light)/ Single layer	No	No	[5]
6.	Gelatin/ PEDOT:PSS	Yes	No	No/No	NA/ Single layer	No	No	[6]
7.	Silk/Fe3O4	No	No	No/Yes	NA / Single layer	No	No	[7]
8.	Starch/GO/ Fe3O4	Yes	No	Yes/Yes	2.5 s / Single layer	No	No	[8]
9.	GO/sodium alginate/Fe3O4	Yes	No	No/Yes	NA / Single layer	No	No	[9]
10.	Gelatin/ PEDOT:PSS/ Fe3O4	Yes	Yes	Yes/Yes	3s (Humidity), 2s (IR-light) / Single layer	Yes	Yes	This work

References

(1) Sun, M.; Wang, P.; Zheng, G.; Dai, K.; Liu, C.; Shen, C. *Soft Matter* **2022**, *18*, 5052–5059.

(2) Xu, M.; Li, L.; Zhang, W.; Ren, Z.; Liu, J.; Qiu, C.; Chang, L.; Hu, Y.; Wu, Y. *Macromolecular Materials and Engineering* **2023**, *308*, 2300200.

(3) Chang, L.; Wang, D.; Huang, Z.; Wang, C.; Torop, J.; Li, B.; Wang, Y.; Hu, Y.; Aabloo, A. *Advanced Functional Materials* **2023**, *33*, 2212341.

(4) Gao, Y.-Y.; Zhang, Y.-L.; Han, B.; Zhu, L.; Dong, B.; Sun, H.-B. *ACS applied materials & interfaces* **2019**, *11*, 37130–37138.

(5) Cheng, X.; Zhao, Q.; Meng, D.; Wang, X.; Ma, J.; Li, J.; He, X. *ACS Applied Polymer Materials* **2021**, *4*, 488–496.

(6) Liu, Y.; Sun, X.-C.; Lv, C.; Xia, H. *Smart Materials and Structures* **2021**, *30*, 125014.

(7) Deng, N.; Li, J.; Lyu, H.; Huang, R.; Liu, H.; Guo, C. *Journal of Materials Chemistry B* **2022**, *10*, 7650–7660.

(8) Chathuranga, H.; Marriam, I.; Chen, S.; Zhang, Z.; MacLeod, J.; Liu, Y.; Yang, H.; Yan, C. *ACS Applied Materials & Interfaces* **2022**, *14*, 16772–16779.

(9) Gao, X.; Zhang, L.; Wang, S.; Yang, T.; Li, H. *ACS Applied Polymer Materials* **2021**, *3*, 4726–4734.